Dynamic Model of Communicating Hydrocephalus for Surgery Simulation

Olivier Clatz, Stéphane Litrico, Hervé Delingette, Nicholas Ayache

INRIA

INSTITUT NATIONAL DE RECHERCHE EN INFORMATIQUE ET EN AUTOMATIQUE

Dynamic Model of Communicating Hydrocephalus for Surgery Simulation

Olivier Clatz — Stéphane Litrico — Hervé Delingette — Nicholas Ayache

N° ????

June 2006

Thème BIO

ISSN 0249-6399 ISRN INRIA/RR--????--FR+ENG

INRIA
SOPHIA ANTIPOLIS

Dynamic Model of Communicating Hydrocephalus for Surgery Simulation

Olivier Clatz, Stéphane Litrico, Hervé Delingette, Nicholas Ayache

Thème BIO — Systèmes biologiques
Projets Asclepios

Rapport de recherche n° ???? — June 2006 — 20 pages

Abstract: We propose a dynamic model of cerebrospinal fluid circulation and intracranial pressure regulation. In this model, we investigate the coupling of biological parameters with a 3D model, to improve the mechanical behavior of the brain in surgical simulators. The model was assessed by comparing the simulated ventricular enlargement evolution with a patient case study of communicating hydrocephalus.

In our model, cerebro-spinal fluid production-resorption system is coupled with a 3D representation of the brain parenchyma. We introduce a new bi-phasic model of the brain tissue allowing for fluid exchange between the brain extracellular space and the venous system. The time evolution of ventricular pressure has been recorded on a symptomatic patient after closing the ventricular shunt. A finite element model has been built based on a CT scan of this patient, and quantitative comparisons between measures and simulated data are proposed.

Key-words: Hydrocephalus, cerebro-spinal fluid, biomechanical model

Unité de recherche INRIA Sophia Antipolis
2004, route des Lucioles, BP 93, 06902 Sophia Antipolis Cedex (France)
Téléphone : +33 4 92 38 77 77 —Télécopie : +33 4 92 38 77 65

Modèle dynamique de l'hydrocéphalie pour la simulation de chirurgie

Résumé : Nous proposons un modèle dynamique de la circulation du liquide céphalorachidien et de la régulation de la pression intracrânienne. Dans ce modèle, nous étudions le couplage entres paramètres biologiques et un modèle 3D, afin d'améliorer le comportement mécanique du cerveau dans les simulateurs de chirurgie. Le modèle a été évalué rétrospectivement en comparant l'évolution de l'élargissement ventriculaire simulé avec celui enregistré chez un patient avec hydrocéphalie communicante.

Dans ce modèle, le système de production résorption du liquide céphalorachidien est couplé avec une représentation 3D du parenchyme cérébral. Nous avons introduis un nouveau modèle bi-phasique du cerveau autorisant l'échange de fluide entre le milieu extracellulaire du cerveau et le système veineux. L'évolution temporelle de la pression ventriculaire a été enregistrée chez un patient symptomatique après fermeture de la dérivation ventriculaire. Un modèle éléments finis a été construit à partir des images tomographiques, et une comparaison entre les mesures et les données simulées est proposée.

Mots-clés : Hydrocépahlie, liquide céphalorachidien, modèle biomécanique

1 Introduction

Different ventriculostomy surgical simulation systems have been developed in the past years. While only considering the geometry of the brain and visual feedback in their early development stages [17], these systems progressively evolved to incorporate force feedback [14,8]. However, none of these system is able to simulate properly the behavior of the brain and its interaction with the cerebro-spinal fluid. We believe the lack of biological relevance of these simulators is a major restriction towards their adoption for training of surgeons.

We propose a dynamic model of cerebrospinal fluid and intracranial pressure regulation, coupling a volumetric biomechanical model with a scalar representation of the CSF circulation. The mathematical simplicity of the interaction of CSF with brain in this model makes it adequate for integration in a surgical simulation system.

Three main components influence ICP: CSF production, circulation, and drainage [3]. The normal CSF dynamics can be described as follow: CSF is mainly produced by the choroid plexus in the lateral and third ventricles. The CSF then flows along the aqueduct of Sylvius, into the fourth ventricle, then through the lateral foramina of Luschka and the medial foramen of Magendie to reach the subarachnoid space. CSF resorption takes place through arachnoid granulations in the sagittal sinus. Recent studies also mention the role of the lymphatic system in CSF drainage [5].

High intraventricular pressure hydrocephalus (as opposed to normal pressure hydrocephalus) are pathological states encountered when CSF circulation or drainage is modified. *Non-communicating* hydrocephalus is characterized by the obstruction of CSF outflow within the ventricular system. Its causes can be congenital or acquired. When the drainage of CSF is obstructed in the sub-arachnoid space (and not in the ventricular system), the hydrocephalus is said to be *communicating*.

Mathematical models of CSF hydrodynamics found in the literature can be classified into two categories: scalar and spatial (2D and 3D) models (see Section 2.1). Scalar models [4,9, 19,23,7] have been used to quantify the CSF outflow resistance or the pressure-volume index, the latter usually with a bolus injection [18,26]. To the best of our knowledge, current spatial models [12, 15] have only considered the non-communicating hydrocephalus. These models always assume that CSF is drained through the brain toward the sub-arachnoid space as a consequence of a pressure gradient in the parenchyma. However, recent experimental studies tend to demonstrate that this hypothesis may not be valid, either in non-communicating or in communicating hydrocephalus [22, 16].

Subarachnoid hemorrhage is the presence of blood within the subarachnoid space, which affects the CSF outflow resistance. As a consequence, the pressure of CSF increases, and ventricles enlarge. The model has been used to simulate hydrocephalus : the temporal evolution of brain deformation and ventricular pressure after closing the shunt are computed. Model parameters have been estimated based on a retrospective case study with pressure measures and images. A quantitative evaluation of the residual error is proposed.

Our contributions with respect to the state of the art are:

- The coupling between a scalar and a 3D spatial model.

- A new conservation equation accounting for the absorption of brain interstitial fluid in the venous system.
- A clinical protocol dedicated to the identification of the model parameters.
- A case study based on a 3D patient-specific model with measures of physiological parameters and a quantitative evaluation of the simulated pathology.

2 Hydrocephalus Models

2.1 Literature Review

There has been significant work aiming at modeling the different phenomena involved in the control of ICP. Two distinct approaches to this problem can be found in the literature [25]:

1. Scalar models. They consist of reducing the CSF production-circulation system to an equivalent hydraulic circuit, governed by scalar equations (capacitances, resistances, etc).
2. Spatial models. They rely on a 2D or 3D model of the brain, often discretized with the finite element method (FEM).

The scalar models usually provide insights into the interaction of CSF with brain, blood vessels, and the rest of the body. Conversely, spatial models give access to a spatial quantification of the local stress, strain, or displacement.

2.1.1 Scalar Models

Hydrocephalus models are closely related to the understanding of the laws governing the ICP. The first representation of the cerebral hydrodynamics was done by Monroe in 1783 [11]. His model was bi-compartmental, only including the CSF and the vessels. His work was later modified by Kellie [6] who added the brain as a deformable compartment to the model, leading to the Monroe-Kellie doctrine:

$$V_{intracranial} = V_{brain} + V_{CSF} + V_{blood} \tag{1}$$

where V_X stands for volume of X. The CSF volume V_{CSF} is divided into the ventricular system and the subarachnoid space. The Monroe-Kellie doctrine simply assumes that the brain, CSF, and blood are enclosed within a rigid shell, so that any increase in volume of one of the compartments implies a decrease of the others.

In this article, we consider that only the lateral ventricles deform, so that the variation of the CSF volume ∂V_{CSF} is equal to the volume variation of the lateral ventricles.

In 1972, Guinane [4] proposed an equivalent circuit analysis of CSF hydrodynamics (Figure 1). The symbol $\ominus$ in Figure 1 represents a perfect flow supply, meaning that the rate of CSF formation in the choroid plexus is assumed to be constant. The symbol $\oplus$

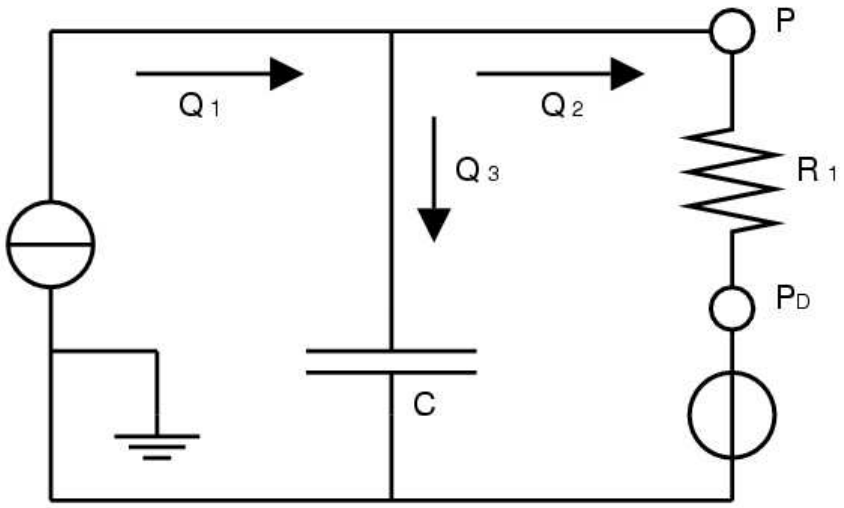

Figure 1: Equivalent circuit analysis of CSF hydrodynamics proposed by Guinane [4].

stands for a perfect pressure supply, equal to the sagittal sinus pressure. CSF hydrodynamics are thus governed by the following equations:

$$Q_1 = Q_2 + Q_3 \tag{2}$$

$$Q_2 = \frac{1}{R_1}(P - P_D) \tag{3}$$

$$Q_3 = C\frac{\partial P}{\partial t} \tag{4}$$

where:

- Q_1, Q_2 and Q_3 are respectively the flow rate of CSF produced in the choroid plexus, absorbed in the venous and lymphatic systems [5], and stored in the ventricles ($Q_3 = \partial V_{CSF}/\partial t$).
- R_1 is the absorption resistance.
- P is the CSF pressure inside the ventricles.
- P_D is a threshold pressure under which the absorption stops (usually taken as the sagittal sinus pressure).

- C is a constant that describes the relationship between the volume V_{CSF} and the pressure P in the ventricles: $C = \partial V_{CSF}/\partial P$.

This model can be simply interpreted. Equation 2 reflects the Monroe-Kellie doctrine, which assumes that the CSF production rate is equal to the sum of the storage rate in the ventricles and the absorption rate in the venous system. Equation 3 states that the CSF rate of absorption is proportional to the pressure difference between the venous system and the CSF pressure, which is a simplification of the Starling hypothesis [21]. Equation 4 links the pressure in the ventricles to their volume.

This system of equations leads to the differential equation:

$$C\frac{\partial P}{\partial t} + \frac{P}{R_1} = Q_1 + \frac{P_D}{R_1} \tag{5}$$

Following the work of Guinane, Marmarou *et al.* [9] proposed a similar equivalent circuit, but changed the constant C in a pressure-dependent function: $C(P) = 1/(kP)$, where k is a constant. Meanwhile, Sklar *et al.* [20] proposed to describe the pressure-volume relationship with the equation $C(P) = 1/(k_1 P + k_2)$. Recently, Sivaloganathan *et al.* [19] showed that any model based on a two compartment assumption (brain and CSF) can be derived from Equation 5 using an appropriate pressure-volume (P-V) relationship:

$$C(P) = \frac{\partial V_{CSF}}{\partial P} \tag{6}$$

As we can see, the compartment models based on the Monroe-Kellie doctrine have been the basis of multiple hydrocephalus models for two centuries. The successive updates mainly consisted in improving the relationship $\partial V_{CSF}/\partial P$, the influence of which is major on the dynamic behavior of the model.

The two-compartment model has only recently been modified to add several additional compartments. In 2000, Stevens *et al.* [23] proposed a four-compartment model that included the rest of the body. This model has been further developed and is now composed of 16 compartments [7].

As a consequence of the increase in complexity, the scalar models are now able to simulate the time variation of scalar measures, and the response to different perturbations (like bolus injections). However, they cannot provide access to local measures in the brain.

2.1.2 Spatial Models

An alternative to the scalar models was proposed by Nagashima *et al.* [12] in 1987 to model a non-communicating hydrocephalus. His 2D model was based on the linear consolidation theory of Biot [2], discretized with the finite element method (FEM). In the linear consolidation theory, the brain is approximated as an elastic porous medium containing CSF in the extracellular space. The CSF flow is then described by Darcy's law:

$$n\left(\underline{v_f} - \underline{v_s}\right) + \underline{\underline{K}}\,\underline{\nabla p} = 0 \tag{7}$$

Where n is the porosity, $\underline{v_f}$ and $\underline{v_s}$ are respectively, the velocities of the fluid and the solid phases (m s^{-1}), $\underline{\underline{K}}$ is the hydraulic permeability (m^4 N^{-1} s^{-1}), and p is the interstitial fluid pressure (N m^{-2}). This model also assumes that volume is conserved, so that the deformation of the solid phase in a control volume is balanced by the sum of the incoming fluid flux to this volume.

The non-communicating hydrocephalus is characterized by the fact that the CSF cannot flow through the main communication pathway: the aqueduct of Sylvius. The authors thus propose to impose a pressure gradient between the ventricles and the cortex as a boundary condition, inducing (as a consequence of Darcy's law, Equation 7) a CSF flux through the brain parenchyma. Note that in this model, the CSF and the extracellular brain fluid are a single phase.

The work of Nagashima *et al.* has been later extended by Peña *et al.* [15] to the study of local measures (void ratio, effective stress, stretch), also on a 2D model. Emphasis has been placed in the work of Peña *et al.* on accuracy and convergence of the discretization method.

Recently, the elastic modulus of the brain parenchyma in the biphasic model has been revised by Taylor *et al.* [24] based on results from the hyper-viscoelastic material model developed by Miller [10]. They concluded that the Young modulus of the brain parenchyma is closer to 600 Pa rather that in the range (3-100 kPa), as proposed in previous studies.

2.2 Proposed Model

2.2.1 Introduction

As presented in Section 2.1, two distinct models -scalar and spatial- have been proposed to model the circulation of CSF in the intracranial space. The weakness of scalar models resides in their inability to describe the expansion of the ventricular wall, or the collapse of the ventricles upon insertion of a shunt. Up to now, the spatial models could not include CSF production and resorption phenomena as boundary conditions. In addition, recent articles tend to demonstrate that the pressure gradient hypothesis may not be valid [16,22].

We propose a new model of communicating hydrocephalus, combining a 3D patient-specific biphasic model of the brain with a scalar description of the CSF production-resorption cycle. We consider the two-compartment model, obeying Equations 2 and 3, and introduce the spatial finite element model to compute the pressure volume relationship.

In this model, the CSF is free to flow through the aqueduct of Sylvius, which is not obstructed. The circulation of CSF through the brain parenchyma and the ventricular wall is thus neglected. The CSF pressure P is different from the brain interstitial fluid pressure p, and the ventricular wall displacement is determined by the effective pressure $P^* = P - p$ on the ventricular wall.

Because the amount of fluid flowing through the brain is very limited in communicating hydrocephalus, we neglect the viscosity of the interstitial fluid, and the pressure gradient induced by Darcy's law 7. Nevertheless, we allow for interstitial fluid exchange with blood through the blood-brain barrier (BBB).

2.2.2 Formulation

Spatial Model We consider the brain to be a biphasic material, composed of an elastic matrix and interstitial fluid, obeying the following quasi-static linear elastic laws:

$$\underline{\underline{\epsilon}} = \frac{1}{2}\left(\underline{\underline{\nabla u}} + \underline{\underline{\nabla u}}^T\right) \quad \text{Strain tensor definition} \tag{8}$$

$$\underline{\underline{\sigma_s}} = \lambda\, tr(\underline{\underline{\epsilon}}) + 2\,\mu\,\underline{\underline{\epsilon}} \quad \text{Constitutive equation} \tag{9}$$

$$\underline{\underline{\sigma}} = \underline{\underline{\sigma_s}} + p\,\underline{\underline{I_3}} \quad \text{Stress tensor definition} \tag{10}$$

$$div\left(\underline{\underline{\sigma}}\right) + \underline{f} = 0 \quad \text{Equilibrium equation} \tag{11}$$

Variables and parameters are defined in Table 1. In this paper, we consider the Young's modulus, E, and Poisson's ratio, ν, to characterize the material. λ and μ are simple functions of these two parameters:

$$\lambda = \frac{E\nu}{(1+\nu)(1-2\nu)}, \qquad \mu = \frac{E}{2(1+\nu)} \tag{12}$$

Symbol	Quantity	Unit
$\underline{\underline{\epsilon}}$	Strain tensor	
$\underline{u}$	Displacement of the solid phase	m
$\underline{\underline{\sigma_s}}$	Effective stress (solid phase)	Pa
λ & μ	Lame elastic & shear modulus	Pa
$\underline{\underline{\sigma}}$	Total stress	Pa
p	Fluid pressure	Pa
$\underline{f}$	External volumetric forces	N m^{-3}

Table 1: Variable and parameters definition

In communicating hydrocephalus, the CSF production-resorption cycle is comparable to the cycle described in Section 1 for the healthy subject, but the hydraulic absorption resistance in the venous system is increased as a consequence of the subarachnoid hemorrhage. The CSF flows through the aqueduct of Sylvius and CSF drainage through the brain is minimal. Thus we propose to neglect the viscous effect of fluid motion in the brain matrix, leading to a constant interstitial pressure, p, in the brain. As a consequence:

$$div\,(p) = 0 \text{ in the brain volume} \tag{13}$$

$$\underline{\underline{\sigma}}\,.\,\underline{n} + p = P \text{ on the ventricular wall} \tag{14}$$

Where $\underline{n}$ is normal to the ventricle surface.

In addition, we allow for fluid exchange between the interstitial space and the blood capillaries in the brain, through the BBB (otherwise, brain could not deform since the interstitial

fluid is incompressible). This absorption flow is considered linear with the pressure difference between the extracellular space and the capillary pressure [21]. The BBB hydraulic resistance is modeled by R_2:

$$\frac{\partial V_{brain}}{\partial t} + \frac{1}{R_2}(p - P_D) = 0 \tag{15}$$

Scalar Model The two-compartment model is used to describe CSF circulation in the intracranial space. This system obeys Equations 2 and 3, leading to the differential equation:

$$\frac{\partial V_{CSF}}{\partial t} + \frac{P}{R_1} = Q_1 + \frac{P_D}{R_1} \tag{16}$$

Combined Model The first term of Equation 16 can be decomposed into:

$$\frac{\partial V_{CSF}}{\partial t} = \frac{\partial V_{CSF}}{\partial P^*}\frac{\partial P^*}{\partial t} \tag{17}$$

Using this formulation, the derivative of the volume of the ventricles with respect to the effective pressure $\partial V_{CSF}/\partial P^*$ can be computed using the FEM. The mechanical model presented in Section 2.2.2 is thus used to discretize the relation between the volume of the ventricles and the effective pressure. This continuous piecewise linear function is defined by the indexed points $\{P_I^*, V_i\}$.

$\partial P^*/\partial t$ can be computed from Equation 15:

$$\frac{\partial P^*}{\partial t} = \frac{\partial (P - p)}{\partial t} = \frac{\partial P}{\partial t} - R_2\frac{\partial Q_3}{\partial t} \tag{18}$$

and, since Q_1 and P_D are constant, $\partial Q_3/\partial t$ can be computed with equations 2 and 3:

$$\frac{\partial Q_3}{\partial t} = -\frac{\partial Q_2}{\partial t} = -\frac{1}{R_1}\frac{\partial P}{\partial t} \tag{19}$$

leading to:

$$\frac{\partial P^*}{\partial t} = \left(1 + \frac{R_2}{R_1}\right)\frac{\partial P}{\partial t} \tag{20}$$

Using this formulation with Equation 16 finally leads to ordinary differential equation:

$$\frac{\partial V_{CSF}}{\partial P^*}\left(1 + \frac{R_2}{R_1}\right)\frac{\partial P}{\partial t} + \frac{1}{R_1}P = Q_1 + \frac{P_D}{R_1} \tag{21}$$

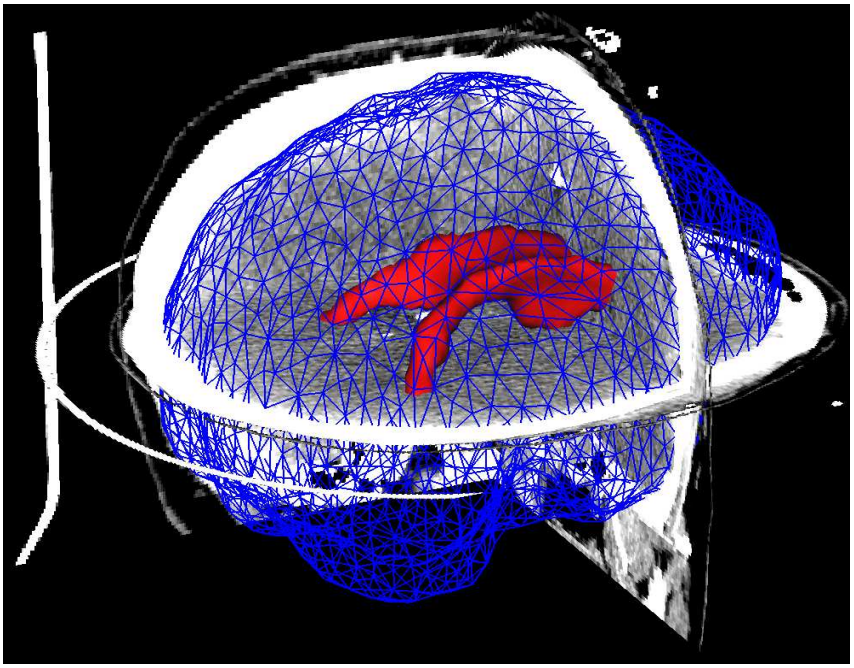

Figure 2: Finite element mesh used for the simulation overlaid on cross sections of the CT scan of the patient (only the cortex and ventricles surfaces are shown).

2.2.3 Boundary Conditions and Time Integration Method

The brain of the patient was first segmented in the images with classical mathematical morphology operations. This segmentation has been meshed with tetrahedra using a state of the art meshing software [13] (17 ,000 vertices, 200 ,000 tetrahedra see Figure 2). The outer surface of the mesh (cortex) is fixed, and we set the pressure P^* in the ventricles.

The mathematical problem has been solved using pre-computation : first, the FEM has been used to compute the displacement of the brain as a piecewise linear function of the effective pressure P^* (more details on the FEM can be found in [1]). Then an analytical method has been used to solve the scalar differential equation 21 describing the ventricular pressure to time function (see Appendix and Algorithm 1 for details). The pre-computation method we used is well suited for real-time surgery simulation. However, the low complexity associated with the coupling of the proposed 2D model makes it also adapted for integration with other numerical schemes.

3 Case Study

3.1 Acquisition Protocol

We propose a clinical protocol designed to identify the characteristic parameters affecting the hydrocephalus. The described protocol does not modify the standard medical and therapeutic follow-up of the patient.

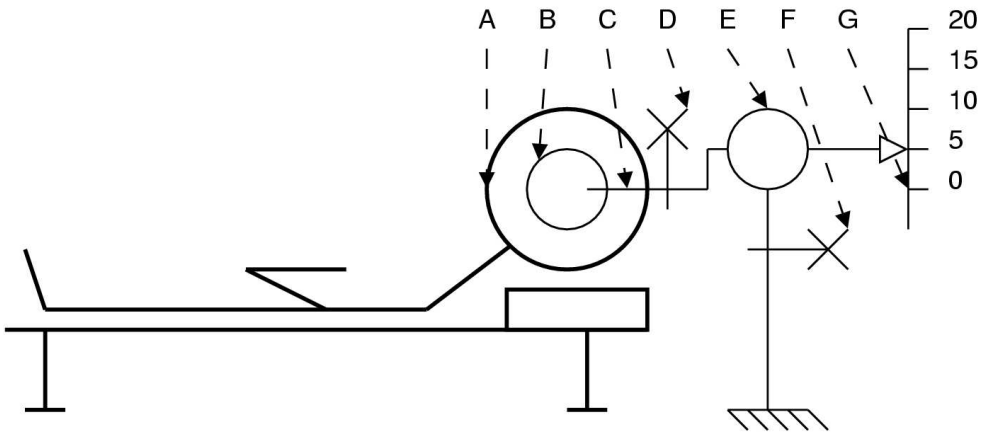

Figure 3: Scheme of the external derivation after the shunt insertion. (A) Head of the patient. (B) Lateral ventricles. (C) Ventricular shunt. (D) Valve. (E) Graduated reservoir. (F) Valve. (G) Reservoir adjustable level (cm).

3.1.1 Population

Our population of interest includes patients presenting a subarachnoid hemorrhage induced by an aneurysm rupture, treated by embolization and requiring an external ventricular shunt. Patients with the following criteria must not be considered for this study: brain hematoma, massive intraventricular hemorrhage, aneurysm treated by surgery, non-treated aneurysm, age under 18 or over 70.

3.1.2 Recorded Parameters

- Volume and shape of the ventricles (with CAT scanner).
- Shunted CSF flow.

- Intraventricular pressure using the pressure sensor of the shunt.

The ventricular shunt is equipped with a reservoir, whose level controls the ventricular pressure (see figure 3). The system is also equipped with two manual valves controlling the shunted flow and the CSF stored in the reservoir.

3.1.3 Measure Acquisitions

After the setup of the shunt, the system is kept open, at the zero level to prevent hypotension in the ventricular system. A first control CAT scan is acquired in this position. The CSF production rate is then recorded every hour, for 24 hours.

After these measures, the shunt is closed. The progressive pressure increase in the ventricles is recorded every ten minutes, until a plateau is reached. Once the steady state is obtained, a second control CAT scan is acquired. The shunt can then be re-opened to evacuate the CSF.

Pressure was recorded 48 hours after shunt insertion. The pathology, characterized by the value of R_1, had already evolved: the steady state pressure after closing the shunt was 1066 Pa (8 mmHg) lower than the pressure measured immediately after shunt insertion.

3.2 Identification of Parameters

The unknowns of our system are R_1, R_2, P_D, Q_1, E, and ν. Two of these parameters are assumed to be constant among patients and are taken from the literature: the sagittal sinus pressure, $P_D = 906$ Pa (6.8 mmHg) [23], and the Poisson's ratio of the brain, $\nu = 0.35$ [24]. Q_1 is directly measured on the graduated reservoir of the shunt every hour. We measured an average CSF production rate $Q_1 = 16$ ml/h. R_1 is computed from the steady state pressure, P_∞, after closing the shunt: $R_1 = (P_\infty - P_D)/Q_1$. To estimate E, we minimize the closest distance $\underline{d}$ between (A) the simulated steady position of the ventricles and (B) the position of the ventricles observed on the CAT image, using a Powell algorithm. The Young's modulus E is then defined as the value that minimizes the sum of this squared distance on the overall ventricular surface Ω:

$$\arg\min_E \int_\Omega \|\underline{d}\| \, d\Omega \tag{22}$$

Finally, the value of R_2 is also estimated with a Powell algorithm, minimizing the squared difference between the simulated pressure evolution and the measured pressure in the ventricles. The computed values are given in table 2.

3.3 Simulation of the Enlargement of the Ventricles

We used the model to simulate the progressive enlargement of ventricles after closing the CSF shunt. In this section, we evaluate and discuss the residual error after optimization of the parameters.

Variable	Value
P_D	906 Pa
P_∞	1729 Pa
ν	0.35
E	7221 Pa
Q_1	16 ml.h^{-1}
R_1	51 Pa.ml^{-1}.h
R_2	16 Pa.ml^{-1}.h

Table 2: Variable Values

First, the displacement error of the ventricle surface was estimated based on the CT scan of the patient and the mesh. The average displacement of the ventricle surface is 2 mm, and the average error computed by the model is 0.8 mm, which is an average relative error of 40%. Figure 5 shows the distribution of this error on the surface of the ventricles. As we can see, the error mainly occurs in high curvature areas, in the occipital horn of the ventricles, where the ventricles do not deform enough. This is also confirmed on Figure 4 (circled area).

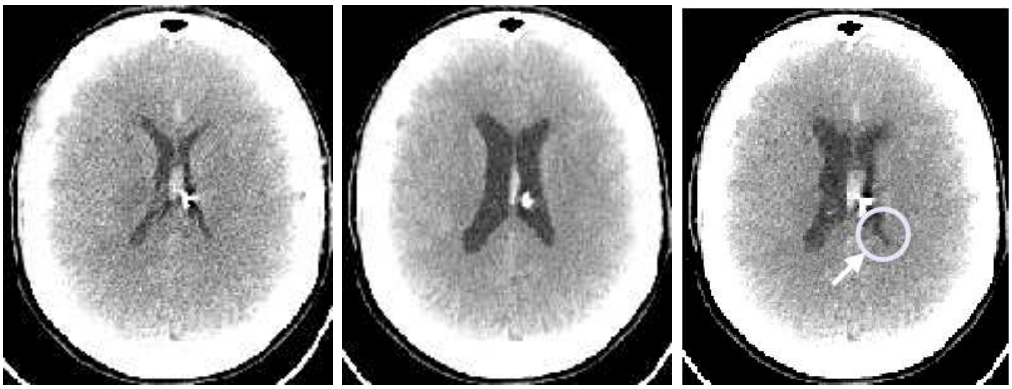

(A) (B) (C)

Figure 4: CT scan of the patient in (A) opened derivation configuration, acquired 1 hour after the procedure and (B) closed derivation configuration, acquired 48 hours after the procedure (steady state). (C) simulated CT scan after model-computed ventricles enlargement (steady state).

Second, we examines the squared difference between the measured time evolution of the ventricular pressure in the patient and the simulated pressure evolution (Figure 6). The average error on measure points is 9%, with a maximum error of 16.2% (60 minutes after closing the shunt).

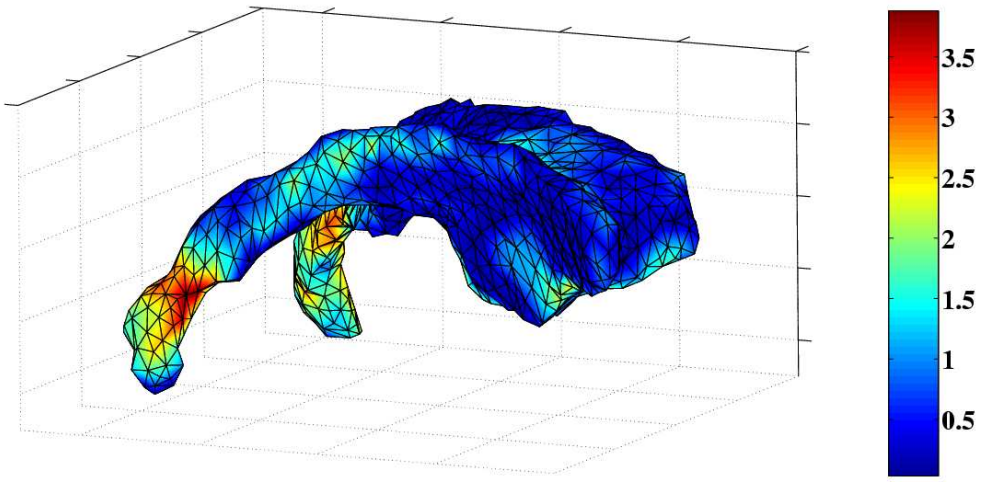

Figure 5: Distribution of the displacement error on the ventricle surface mesh (mm).

We identify the following remaining error sources:

- The segmentations of the ventricles may be inaccurate. This is all the more critical that both the error criteria and the mesh are based on these segmentations. In particular, if the ventricles are very contracted, as on the open shunt configuration image (panel A of Figure 4), part of the ventricle can be missed by the segmentation leading to the undeformed part of the ventricle (circled area in panel C of Figure 4).
- The linear model may show some limitations in the horn of the ventricles. This error source can be of even greater importance for patient with more acute hydrocephalus.
- The influence of blood vessels in the brain is not taken into account. In particular, the auto-regulation of blood pressure might be able to explain the rebound observed on the pressure to time evolution (Figure 6).
- The pressure measure sample rate is too low and transient phenomena might be missed. The measures should be recorded with a higher frequency (at least every minute). Ideally, an automatic system should be used to record this pressure.

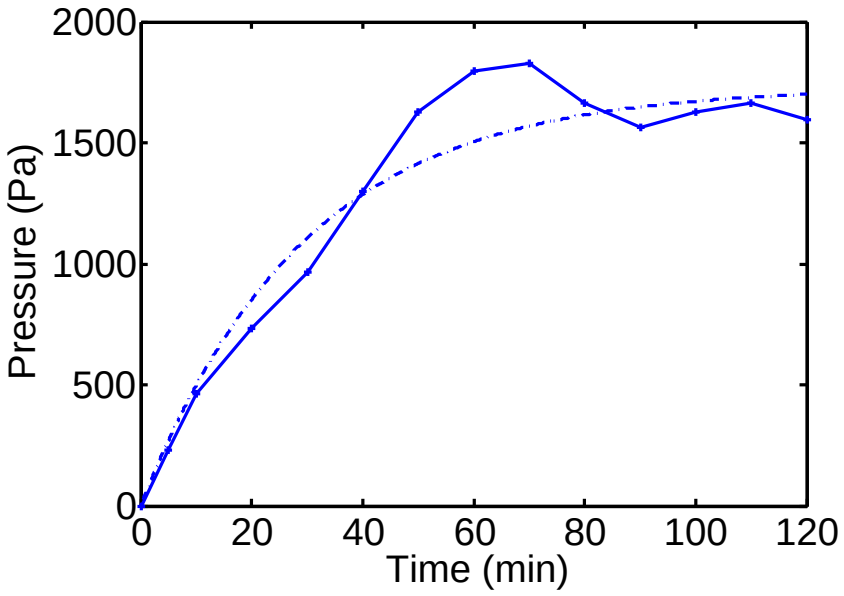

Figure 6: Evolution of the ventricular pressure as a function of time after closing the shunt. Continuous line: Measure on the patient. Dashed line: Simulated pressure increase with the model.

4 Conclusion

We proposed in this article a new model of hydrocephalus, which couples a 3D representation of the brain parenchyma with a scalar hydraulic description of the CSF circulation in the intracranial space. The link between the scalar and the 3D model has been made through the relation $\partial V_{CSF}/\partial P^*$, which makes this model amenable to further improvements, either of the mechanical constitutive equation (including a non linear relation, for example), or of the scalar model (incorporating additional electric equivalent components).

The current model revokes the assumption that the brain is incompressible, and allows for brain extracellular fluid exchange with the blood. Contrary to previous spatial models, our model does not assume that CSF is drained through the brain. As a consequence, we make the assumption that interstitial fluid viscosity can be neglected, leading to a brain pressure in agreement with the recent in-vivo measurements [22, 16].

This model now provides a useful tool to study the influence of the pathology on the evolution of local parameters (local brain compression, perfusion pressure, etc) based on the

patient geometry and using global physiological measures. In addition, we made quantitative measures of the model accuracy, which will facilitate the comparison with future models.

A Analytical Integration in Time of Equation 21

Using the FEM, we can compute a piecewise linear function $\partial V_{CSF}/\partial P^*$. Its associated computation points are defined by indexed pairs $\{P_i^*, V_i\}$. We define $\alpha_i = (\partial V_{CSF}/\partial P^*)_i = \left(V_{i+1} - V_i\right) / \left(P_{i+1}^* - P_i^*\right)$. The solution $P(t)$ of Equation 21 is successively computed on intervals $[T_i,\, T_{i+1}]$. The general solution of Equation 21 for $t \in [T_i,\, T_{i+1}]$ takes the form:

$$P\left(t\right) = P_\infty + \left(P_i - P_\infty\right) \exp - \frac{t - T_i}{\alpha_i \left(R_1 + R_2\right)} \tag{23}$$

with $P_\infty = Q_1 R_1 + P_D$.

The P_i are computed using the relation $P^* = P - p$:

$$\begin{aligned} P_i &= P(T_i) = P_i^* + p_i && (24)\\ &= P_i^* + P_D + R_2 Q_3 && (25)\\ &= P_i^* + P_D + R_2 \left(Q_1 - \frac{P_i - P_D}{R_1}\right) && (26)\\ \Rightarrow\ P_i &= \frac{R_1}{R_1 + R_2}\left(P_i^* + R_2 Q_1\right) + P_D && (27) \end{aligned}$$

And the integration time steps T_i are recursively computed using the continuity relation, $P_{i+1} = P(T_{i+1})$:

$$P_{i+1} = P_\infty + \left(P_i - P_\infty\right) \exp - \left(\frac{T_{i+1} - T_i}{\alpha_i \left(R_1 + R_2\right)}\right) \tag{28}$$

So that:

$$T_{i+1} = T_i + \alpha_i \left(R_1 + R_2\right) \ln \left(\frac{P_\infty - P_i}{P_\infty - P_{i+1}}\right) \tag{29}$$

The overall computation of the time evolution of the ventricular pressure is presented in Algorithm 1.

Algorithm 1 Computation of the time evolution of the ventricular pressure

Get the pressure step ΔP from user
$i = 0;\ T_0 = 0;\ P_0 = 0$
while $P < P_\infty$ **do**
  $P_{i+1} = P_i + \Delta P$
  Compute P_i^* from Equation 27
  $i = i + 1$
end while
$i_{max} = i$
for $i = 0;\ i < i_{max};\ i = i + 1$ **do**
  Compute V_i from P_i^* with the FEM
end for
for $i = 0;\ i < i_{max};\ i = i + 1$ **do**
  Compute T_{i+1} from Equation 29
  for $t \in [T_i T_{i+1}]$, Compute $P(t)$ from Equation 23
end for

References

[1] K.J. Bathe. *Finite Element Procedures in Engineering Analysis*. Prentice-Hall, Englewood Cliffs, N.J, 1982.

[2] M.A. Biot. General theory of three-dimensional consolidation. *Journal of Applied Physics*, (12):155–164, 1941.

[3] Marek Czosnyka, Zofia Czosnyka, Shahan Momjian, and John D Pickard. Cerebrospinal fluid dynamics. *Physiol Meas*, 25(5):51–76, Oct 2004.

[4] J.E. Guinane. An equivalent circuit analysis of cerebrospinal fluid hydrodynamics. *Am J Physiol.*, 223(2):425–30, Aug 1972.

[5] M. Johnston and C. Papaiconomou. Cerebrospinal fluid transport: a lymphatic perspective. *News in Physiological Sciences*, 17(6):227–30, Dec. 2002.

[6] G. Kellie. An account of the appearances observed in the dissection of two of three individuals presumed to have perished in the storm of the 3d, and whose bodies were discovered in the vicinity of leith on the morning of the 4th of november 1821 with some reflections on the pathology of the brain. *Trans Med Chir Sci Edinb*, (1):84–169, 1824.

[7] W.D. Lakin, S.A. Stevens, B.I. Tranmer, and P.L. Penar. A whole-body mathematical model for intracranial pressure dynamics. *J Math Biol.*, 46(4):347–83, Apr 2003.

[8] C Luciano, P Banerjee, G M Lemole, and F Charbel. Second generation haptic ventriculostomy simulator using the immersivetouch(tm) system. *Stud Health Technol Inform*, 119:343–348, 2005.

[9] A. Marmarou, K. Shulman, and R. Rosende. A nonlinear analysis of the cerebrospinal fluid system and intracranial pressure dynamics. *J Neurosurg.*, (48):530–537, 1978.

[10] K. Miller. *Biomechanics of Brain for Computer Integrated Surgery*. Warsaw University of Technology Publishing House, 2002.

[11] A. Monroe. Observations on the structure and function of the nervous system. Creech & Johnson, Edinburgh, 1783.

[12] T. Nagashima, N. Tamaki, S. Matsumoto, B. Horwitz, and Y. Seguchi. Biomechanics of hydrocephalus: A new theoretical model. *Neurosurgery*, 21(6):898–904, 1987.

[13] S. Oudot, L. Rineau, and M. Yvinec. Meshing volumes bounded by smooth surfaces. Research report 5626, INRIA, 2005.

[14] B Panchaphongsaphak, D Stutzer, E Schwyter, R L Bernays, and R Riener. Haptic device for a ventricular shunt insertion simulator. *Stud Health Technol Inform*, 119:428–430, 2005.

[15] A. Peña, M.D. Bolton, H. Whitehouse, and J.D. Pickard. Effects of brain ventricular shape on periventricular biomechanics: A finite-element analysis. *Neurosurgery*, 45(1):531–538, 1999.

[16] Richard D. Penn, Max C. Lee, Andreas A. Linninger, Keith Miesel, Steven Ning Lu, and Lee Stylos. Pressure gradients in the brain in an experimental model of hydrocephalus. *J Neurosurg*, 102(6):1069–1075, Jun 2005.

[17] N I Phillips and N W John. Web-based surgical simulation for ventricular catheterization. *Neurosurgery*, 46(4):933–936, Apr 2000.

[18] K. Shapiro and A. Marmarou. Clinical applications of the pressure-volume index in treatment of pediatric head injuries. *J Neurosurg*, 56(6):819–25, 1982.

[19] S. Sivaloganathan, G. Tenti, and J. M. Drake. Mathematical pressure volume models of the cerebrospinal fluid. *Appl. Math. Comput.*, 94(2-3):243–66, 1998.

[20] F. H. Sklar, C. W. Beyer Jr, and W. K. Clark. Physiological features of the pressure-volume function of brain elasticity in man. *J Neurosurg*, 53(2):166–172, Aug 1980.

[21] F. Starling. On the absorption of fluids from the connective tissue spaces. *Journal of Physiology*, 19:312–326, 1896.

[22] Hannes Stephensen, Magnus Tisell, and Carsten Wikkelso. There is no transmantle pressure gradient in communicating or noncommunicating hydrocephalus. *Neurosurgery*, 50(4):763–771, Apr 2002.

[23] S.A. Stevens and W.D. Lakin. Local compliance effects on the global csf pressure-volume relationship in models of intracranial pressure dynamics. *Mathematical and Computer Modeling of Dynamical Systems*, 6(4):445–465, 2000.

[24] Z. Taylor and K. Miller. Reassessment of brain elasticity for analysis of biomechanisms of hydrocephalus. *Journal of Biomechanics*, 37(8):1263–1269, Aug 2004.

[25] G. Tenti, J. M. Drake, and S. Sivaloganathan. Brain biomechanics: mathematical modeling of hydrocephalus. *Neurological Research*, (22):19–24, 2000.

[26] M. Ursino and C. A. Lodi. A simple mathematical model of the interaction between intracranial pressure and cerebral hemodynamics. *J Appl Physiol*, 82(4):1256–1269, Apr 1997.

Contents

Unité de recherche INRIA Sophia Antipolis
2004, route des Lucioles - BP 93 - 06902 Sophia Antipolis Cedex (France)

Unité de recherche INRIA Futurs : Parc Club Orsay Université - ZAC des Vignes
4, rue Jacques Monod - 91893 ORSAY Cedex (France)
Unité de recherche INRIA Lorraine : LORIA, Technopôle de Nancy-Brabois - Campus scientifique
615, rue du Jardin Botanique - BP 101 - 54602 Villers-lès-Nancy Cedex (France)
Unité de recherche INRIA Rennes : IRISA, Campus universitaire de Beaulieu - 35042 Rennes Cedex (France)
Unité de recherche INRIA Rhône-Alpes : 655, avenue de l'Europe - 38334 Montbonnot Saint-Ismier (France)
Unité de recherche INRIA Rocquencourt : Domaine de Voluceau - Rocquencourt - BP 105 - 78153 Le Chesnay Cedex (France)

Éditeur
INRIA - Domaine de Voluceau - Rocquencourt, BP 105 - 78153 Le Chesnay Cedex (France)
http://www.inria.fr
ISSN 0249-6399